COMMUN. MATH. SCI.
Vol. 8, No. 2, pp. 601–626

THE EXACT EVOLUTION OF THE SCALAR VARIANCE IN PIPE AND CHANNEL FLOW*

ROBERTO CAMASSA†, ZHI LIN‡, AND RICHARD M. MCLAUGHLIN§

Dedicated to the sixtieth birthday of Professor Andrew Majda

Abstract. In 1953 G.I. Taylor showed theoretically and experimentally that a passive tracer diffusing in the presence of laminar pipe flow would experience an enhanced diffusion in the longitudinal direction beyond the bare molecular diffusivity, κ, in the amount $\frac{a^2U^2}{192\kappa}$, where a is the pipe radius and U is the maximum fluid velocity. This behavior is predicted to arise after a transient timescale $\frac{a^2}{\kappa}$, the diffusive timescale for the tracer to cross the pipe. Typically, κ is very small, so provided a fairly long time has passed, this is a very large diffusive boost. Before this timescale, the evolution is expected to be anomalous, meaning the scalar variance does not grow linearly in time. A few attempts to compute this anomalous growth have been made in the literature for different special cases with different approximations. Here, we derive an exact approach which provides the scalar variance evolution valid for all times for channel and pipe flow for the case of vanishing Neumann boundary conditions. We show how this formula limits to the Taylor regime, and rigorously study the anomalous regime for a range of initial data. We find that the anomalous timescales and exponents depend strongly upon the form of the data. For initial data whose transverse variation is a delta function on the centerline, the anomalous regime emerges after a timescale, $(\frac{a^4}{\kappa U^2})^{\frac{1}{3}}$, with variance growing as t^α, with $\alpha=4$. In contrast, for the case of uniform data (independent of the transverse variable), the anomalous timescale is $\frac{\kappa}{U^2}$, with exponent $\alpha=2$, and this result is generalized for generic shear flows given that the initial condition is not a transverse Dirac delta function. Further, these exact formulas explicitly show what features the short time approximations which ignore physical boundaries are able to capture.

Key words. Taylor dispersion, mixing, transport, stochastic and partial differential equations, multi-scale asymptotics, pipe and channel flow.

AMS subject classifications. 82C70, 82C31, 34E13.

1. Introduction

The enhanced diffusion of a passive scalar is a fundamental problem with a long history, dating back to the pioneering work of G.I. Taylor [18] who developed the first theory and experiments for pipe flow, for which the phrase Taylor dispersion was born. Taylor dispersion is the phenomena by which a shear flow boosts the longitudinal diffusivity well above the bare molecular diffusivity, κ; on long times Taylor theoretically predicted and experimentally validated this diffusivity to be $\kappa(1+\frac{U^2a^2}{192\kappa^2})$ for the case of laminar flow in a pipe, where U is the maximum velocity and a is the pipe radius.

Since Taylor, there has been an intense effort to calculate, the general enhanced diffusion coefficient for a given fluid flow, which is known to be a complicated function of the fluid flow structure as well as of the Peclet number, $\mathrm{Pe}=\frac{Ua}{\kappa}$, where U and a are typical flow and length scales. Much of this effort has been explored using the multi-scale asymptotic method of homogenized averaging theory, just one of the many tools Andy Majda has employed in his many studies in this area of his influential research

*Received: October 30, 2008; accepted (in revised version): July 16, 2009.

†Department of Mathematics, University of North Carolina, Chapel Hill, NC 27599, USA (camassa@email.unc.edu).

‡Department of Mathematics, University of Michigan, Ann Arbor, MI 48109, USA (linzhi@umich.edu).

§Department of Mathematics, University of North Carolina, Chapel Hill, NC 27599, USA (rmm@email.unc.edu).

program (see the review article at Physics Reports for a thorough overview of modern turbulent transport) [15].

While Taylor's work and the turbulent transport campaign have been quite successful in predicting the long time transport behavior, and in generally assessing how the emergence of stochasticity in turbulent fluid flows manifests upon transported quantities with and without sufficient scale separation [3, 4, 15], much less is generally known regarding transient dynamics, which may be highly anomalous, and even less is known with the inclusion of real, solid wall boundary conditions. It is for this reason that we revisit the cases of channel and pipe flow with the goal of capturing the exact evolution using the correct physical boundary conditions for confined geometries.

Some transient predictions have been obtained for the case of pipe flow, mainly using various free space approximations; see Young and Jones for a partial listing of the known results on Taylor dispersion [20]. By assuming the tracer does not interact with the pipe wall, Lighthill peered into the anomalous regime, and found that a transversely uniform distribution of scalar would spread longitudinally with variance growing quadratically in time [11]. More recently, in an interesting study Latini and Bernoff generalized the method employed by Lighthill to consider the anomalous spread of an initial distribution, which is a delta function in the transverse direction, again employing a free space approximation neglecting the pipe wall boundary [8]. Their results predict an anomalous scaling regime in which the scalar variance grows with scaling exponents and timescales depending upon the location of the transverse delta function relative to the centerline of the pipe, while all of these free space approaches break down when the pipe wall begins to influence the evolution.

A few other studies regarding transient phenomena en route to Taylor's enhanced diffusion regimes merit mention. Aris [1] succeeded using a moment method to compute the mean tracer distribution for all times for the special case of an initial tracer which is uniformly distributed in the transverse direction. Chatwin [6] generalized the Aris result for transversely uniform initial data to the full variance temporal evolution, and computed short time asymptotic behavior of this special case. Furthermore by using a similar formal expansion Chatwin provided the full time behavior for a some additional forms of smooth initial data. By employing an approach based on the stochastic differential equations of the underlying passive scalar, Vanden-Broeck [19] studied a more general class of time varying shear layers. In particular, he rederived the variance formula obtained by Chatwin for the case of transversely uniform initial data. Finally, Smith [17] improved upon Chatwin's approach employing a formal Gaussian-Hermite ansatz to obtain a general formula for the temporal variance evolution with transverse delta function initial data. While these studies succeed in computing formulas for the scalar variance in various setups at various levels of accuracy, the results of our paper, which include the general, mathematically rigorous, short time asymptotic behavior of the scalar variance, and specifically the prediction of the anomalous timescales for arbitrary initial data, appears to have not been previously explored.

Our approach employs the stochastic differential equations underlying the passive scalar equation, with care paid in properly imposing the vanishing Neumann conditions for all time at the pipe wall. For the case of channel and pipe flow, the random trajectories of these equations may be calculated exactly in closed form. In turn, statistical moments may be obtained by appealing to two key tools: first, the exact Green's function is available for the heat equation in a circular pipe or finite channel

subject to vanishing Neumann boundary conditions. This provides the single point probability density function for bounded Brownian motion for these geometries. Second, the application of rules of conditional probability provides the means to compute the necessary higher order temporal correlations needed to explicitly calculate, with no approximations, the moments needed to construct the scalar variance. This gives rise to an explicit elementary formula for the evolution of the scalar variance for a large class of initial distributions (radially symmetric in the case of pipe flow). These formulas provide rigorous short and long time asymptotics which show the emergence of anomalous scaling regimes in which the scalar variance is seen to demonstrate nonlinear, algebraic growth and generally shows the universality of the Taylor timescale, a^2/κ. The anomalous scaling regimes (both timescale and exponent) can further be seen to depend nontrivially on the form of the initial data's transverse dependence.

The paper is organized as follows: in section 2, we provide a review of the various long time limits which may be obtained using multi-scale asymptotics for both pipe and channel flow to compute the effective diffusivities. In section 3, we study the stochastic differential equation for the case of channel flow, while in section 4, we turn to the stochastic differential equation for pipe flow. In both cases, we compute the complete variance valid for all times. The long time limit of the variance is shown to agree precisely with the multi-scale calculations in all cases. The particularly interesting simplifying case of transversely uniform data for both pipe and channel flow is examined in detail. In these cases, complete short and long time asymptotic expansions for the variance are computed which show the explicit form of the anomalous regime. In contrast, the situations with more general initial data are studied for two different flow geometries which involve delta functions in both the longitudinal and spanwise directions. Through these cases, we have rigorously shown that the anomalous regime depends non-trivially upon the form of the initial data, changing both the anomalous timescales and scaling exponents. To further probe this dependence, for the case of 2D channel flow, we consider an initial condition which is a delta function in the longitudinal direction and a centered box function in the transverse direction to explore how the case with transversely uniform initial data arises. At the end of section 4, we show how the variance predicted by Latini and Bernoff using free space methods arises directly from the stochastic differential equation approach by simply replacing the bounded Brownian motion with free space Brownian motion. We explore how the free space methodology successfully captures the anomalous regime provided the transverse delta function initial condition is sufficiently isolated from the wall, and document how those predictions erode as the source line is moved closer to the wall. Additionally, using this free space approach we establish that the short time asymptotic variance correction to the diffusive regime is always quadratic in time for generic steady shear flows provided the initial condition is not a Dirac delta in the transverse direction. In section 5 higher order statistics are discussed, and, in particular, the evolution of the skewness is studied with Monte Carlo simulations. This shows how the anomalous and Taylor timescales for channel flow computed for the scalar variance precisely match the timescales on which the scalar experiences a non-zero, transient skewness. Lastly, some details regarding the moment calculations and Monte Carlo method are presented in the Appendix.

2. The multiscale analysis approach

We now review the multi-scale asymptotic calculation which yields the effective diffusivities for the two cases of pipe and channel flow, assuming a scale separation in the initial data, which is expected after a long time has passed.

Consider the following advection-diffusion equation:

$$\begin{cases} \dfrac{\partial T}{\partial t} + u(y,z)\dfrac{\partial T}{\partial x} = \kappa \Delta T, \\ \lim_{|x|\to\infty} T = 0,\ \dfrac{\partial T}{\partial \vec{n}}\Big|_{\partial\Omega} = 0, \\ T(x,y,z,t=0) = T_d\left(\dfrac{x}{L}\right), \end{cases} \tag{2.1}$$

where the domain Ω can be either of the following:

$$\Omega = \begin{cases} \{(x,y,z)|y^2+z^2=a^2\}, & \text{Pipe Geometry}, \\ \{(x,y,z)|y\in[0,a],\} & \text{Channel Geometry}, \end{cases} \tag{2.2}$$

and the parabolic shear u is accordingly

$$u(y,z) = \begin{cases} U\Big(\dfrac{1}{2} - \dfrac{y^2+z^2}{a^2}\Big), & \text{Pipe Geometry;} \\ 4U\Big[\dfrac{z}{a}(1-\dfrac{z}{a}) - \dfrac{1}{6}\Big], & \text{Channel Geometry.} \end{cases} \tag{2.3}$$

Here we use the centerline, maximum velocity as the characteristic velocity U and we make a Galilean translation in the x-direction as mentioned earlier, so that the average shear over the transverse plane has mean zero. Also, the length scale $L \gg a$ is chosen since we are only interested in the diffusing behavior in the x-direction at large times, when the scalar in the transverse directions is well-mixed and can be considered uniform.

With the change of variables

$$\begin{gathered} x' = \frac{x}{L}, \quad y' = \frac{y}{a}, \quad z' = \frac{z}{a}, \quad t' = \frac{\kappa}{a^2}t, \\ T(x,y,z,t) = T'(x',y',z',t'), \quad u(y,z) = u'(y',z'), \end{gathered} \tag{2.4}$$

we can drop the primes without confusion and obtain the nondimensionalized equation for (2.1):

$$\begin{cases} \dfrac{\partial T}{\partial t} + \dfrac{\mathrm{Pe}}{\varepsilon}u(y,z)\dfrac{\partial T}{\partial x} = \dfrac{\partial^2 T}{\partial x^2} + \dfrac{1}{\varepsilon^2}\big(\dfrac{\partial^2 T}{\partial y^2} + \dfrac{\partial^2 T}{\partial z^2}\big), \\ \lim_{|x|\to\infty} T = 0,\ \dfrac{\partial T}{\partial \vec{n}}\Big|_{\partial\Omega} = 0, \\ T(x,y,z,t=0) = T_d(x). \end{cases} \tag{2.5}$$

Here we introduce the Péclet number and the scale separation as

$$\mathrm{Pe} = \frac{Ua}{\kappa}, \quad \varepsilon = \frac{a}{L}. \tag{2.6}$$

Pe characterizes the relative importance of advection to molecular diffusion and ε compares the length scales in the transverse and flow directions. Furthermore, the fluid domain (2.2) and the shear flow (2.3) can also be nondimensionalized accordingly.

Next, we seek the asymptotic approximation to $T(x,y,z,t)$ in the limit $\varepsilon \to 0$ that has the following multiscale expansion

$$T(x,y,z,t) = T_0(x,\xi,y,z,t) + \varepsilon T_1(x,\xi,y,z,t) + \varepsilon^2 T_0(x,\xi,y,z,t) + O(\varepsilon^3) \tag{2.7}$$

with two spatial scales in x-direction: x (slow) and $\xi = \frac{x}{\varepsilon}$ (fast). Consequently, the differential operators along the x-direction will be replaced:

$$\frac{\partial}{\partial x} \to \frac{\partial}{\partial x} + \frac{1}{\varepsilon}\frac{\partial}{\partial \xi}, \quad \frac{\partial^2}{\partial x^2} \to \frac{\partial^2}{\partial x^2} + \frac{2}{\varepsilon}\frac{\partial^2}{\partial x \partial \xi} + \frac{1}{\varepsilon^2}\frac{\partial^2}{\partial \xi^2}. \tag{2.8}$$

Substituting (2.7) and (2.8) into equation (2.5), we would have a hierarchy of equations, as one would see in a classical *Homogenization Problem*, such that the following equation holds for arbitrarily small ε,

$$O(\varepsilon^{-2}): \qquad \mathcal{L}T_0 := \Big[\mathrm{Pe}\, u(y,z)\frac{\partial}{\partial \xi} - \left(\frac{\partial^2}{\partial \xi^2} + \frac{\partial^2}{\partial y^2} + \frac{\partial^2}{\partial z^2}\right)\Big] T_0 = 0. \tag{2.9}$$

Since the initial condition, T_d, is a function of the large-scale variable x only, we expect the leading behavior of the solution to be a function of x and t, namely, $T_0(x,\xi,y,z,t) = T_0(x,t)$ which is consistent with the above equation,

$$O(\varepsilon^{-1}): \qquad \mathcal{L}T_1 = -\mathrm{Pe}\, u(y,z)\frac{\partial T_0}{\partial x} + 2\frac{\partial^2 T_0}{\partial x \partial \xi}. \tag{2.10}$$

Fredholm's Alternative requires that this equation has a solution if and only if the average of right hand side over the transverse directions (y and z), $\langle\cdot\rangle$, vanishes, which is guaranteed since $\langle u(y,z)\rangle$ and $\frac{\partial^2 T_0}{\partial x \partial \xi} = 0$. For example, in the channel geometry

$$\big\langle u(y,z)\big\rangle = 4U\int_0^1 \Big[z(1-z) - \frac{1}{6}\Big]dz = 4U\left(\frac{1}{2} - \frac{1}{3} - \frac{1}{6}\right) = 0. \tag{2.11}$$

Therefore, introducing the separation of variables $T_1(x,\xi,y,z,t) = \dfrac{\partial T_0}{\partial x}\theta(\xi,y,z) + C(x,t)$, we obtain the *cell problem*:

$$\mathcal{L}\theta = -\mathrm{Pe}\, u, \qquad \frac{\partial \theta}{\partial \vec{n}}\Big|_{\partial\Omega} = 0. \tag{2.12}$$

Since neither the right hand side nor the boundary condition depends on ξ, a particular solution to this PDE in the pipe case is

$$\theta(\xi,y,z) = \overline{\theta}(r) = \mathrm{Pe}(\Delta_r)^{-1}u(r), \tag{2.13}$$

where $r = \sqrt{y^2+z^2}$ and $\Delta_r = \frac{\partial}{r\partial r}(r\frac{\partial}{\partial r})$ is the cylindrical Laplacian operator with periodic boundary conditions in the longitudinal direction and the Neumann boundary condition in (2.12). In the channel case, the solution is even more straightforward: $\theta(\xi,y,z) = \theta(z) = \mathrm{Pe}\big(\frac{\partial^2}{\partial z^2}\big)^{-1}u(z)$, since the channel shear in (2.3) only depends on z.

$$O(\varepsilon^0): \qquad \mathcal{L}T_2 = -\frac{\partial T_0}{\partial t} - \mathrm{Pe}\, u(y,z)\frac{\partial T_1}{\partial x} + \frac{\partial^2 T_0}{\partial x^2} + 2\,\frac{\partial^2 T_1}{\partial x \partial \xi}. \tag{2.14}$$

The last term on the right hand side indeed vanishes since T_1 does not depend on ξ as we discussed. Another application of Fredholm's Alternative yields the *homogenized/effective diffusion equation* in the x-direction:

$$\frac{\partial T_0}{\partial t} = \Big(1 - \mathrm{Pe}\big\langle u\theta\big\rangle\Big)\frac{\partial^2 T_0}{\partial x^2}. \tag{2.15}$$

From (2.3) and (2.12)–(2.15), the diffusion enhancement in the pipe geometry is

$$\begin{aligned}
-\langle u\theta\rangle &= -\frac{\mathrm{Pe}}{\pi}\int_0^{2\pi} d\phi \int_0^1 r\,u(r)\bar{\theta}(r)dr \\
&= -2\int_0^1 r\theta\Big[\frac{\partial}{r\partial r}\big(r\frac{\partial\theta}{\partial r}\big)\Big]\,dr \\
&= -2r\theta\frac{\partial\theta}{\partial r}\Big|_{r=0}^{r=1} + 2\int_0^1 r\Big(\frac{\partial\theta}{\partial r}\Big)^2 dr \\
&= 2\mathrm{Pe}^2\int_0^1 r\Big[\frac{1}{r}\int_0^r s\big(\frac{1}{2}-s^2\big)ds\Big]^2 dr \\
&= \frac{\mathrm{Pe}^2}{192},
\end{aligned} \tag{2.16}$$

whereas in the channel geometry,

$$-\mathrm{Pe}\langle u\theta\rangle = -\int_0^1 \theta\frac{\partial^2\theta}{\partial z^2}dz = \mathrm{Pe}^2\int_0^1\Big\{\int_0^z 4\big[s\big(1-s\big)-\frac{1}{6}\big]ds\Big\}^2 dz = \frac{2\mathrm{Pe}^2}{945}. \tag{2.17}$$

Consequently, in either geometry, the enhanced diffusivity can be defined as

$$\kappa_{\mathrm{eff}} := \kappa\big(1-\mathrm{Pe}\langle u\theta\rangle\big) = \kappa\big(1+\mathcal{C}\mathrm{Pe}^2\big) \tag{2.18}$$

in the limit $\varepsilon\to 0$ [1, 18], or sufficiently, $t\to\infty$, where $\mathcal{C}=\mathcal{C}_p=1/192$ in a pipe and $\mathcal{C}=\mathcal{C}_c=2/945$ in a channel. This result suggests that to the leading order, the flow-induced enhancement scales *quadratically* with the Péclet number with a constant factor at large times. This is exactly the classical result for Taylor dispersion [18, 8].

From the above calculations, it is clear that the multiscale analysis above rests on the scale separation between the initial scalar distribution of the scalar and the flow geometry. With other types of data, such as point sources that do not possess scale separations, an extra, fast timescale needs to be introduced [10] and similar analysis would also produce the description for the long-time and large spatial scale features of the passive scalar field. In the next section, we will propose a general SDE formulation that yields the same results and can solve a much wider class of problems while revealing their transient dynamics in a straightforward way.

3. The stochastic differential equation approach: channel flow

From the previous section, the homogenization analysis does reveal the long time limit of the flow-enhanced diffusion as a leading order solution. However, as we will demonstrate next, a study of the *stochastic differential equation* representation of equation (2.1) can actually obtain explicit formulas for the diffusion enhancement valid for arbitrary times and for arbitrary initial distributions.

3.1. The Green's function for the two-dimensional channel. In working with the stochastic differential equation, we will need the explicit Green's function for the infinite strip with vanishing Neumann boundary conditions. Here, for completeness, we present this formula, which will be essential in providing the single point statistics for the bounded Brownian motions.

Consider the fundamental solution to the nondimensional diffusion equation for

a passive scalar in an infinitely long, two-dimensional channel:

$$\begin{cases} \dfrac{\partial}{\partial\tau}G(x',z',\tau)=\Delta G(x',z',\tau), \quad (x,z)\in(-\infty,\infty)\times(0,1), t>0, \\ \lim_{|x|\to\infty}G=0,\ \dfrac{\partial G}{\partial z}\Big|_{z'=0,1}=0, \\ G(x',z',\tau=0)=\delta(x'-X_0')\delta(z'-Z_0'). \end{cases} \tag{3.1}$$

where nondimensional variables x', X_0', z', Z_0', τ are related to the dimensional size of the channel a, molecular diffusivity κ, and the dimensional variables x, X_0, z, Z_0, t by

$$x'=\frac{x}{a}, \quad z'=\frac{z}{a}, \quad X_0'=\frac{X_0}{a}, \quad Z_0'=\frac{Z_0}{a}, \quad \tau=\frac{\kappa t}{a^2}. \tag{3.2}$$

Without confusion, we will drop the $'$ in the spatial variables hereafter. After the Fourier transform in x and the cosine series expansion in z, namely,

$$G(x,z,\tau)\to\hat{G}_n(k,\tau)=\sqrt{\frac{2}{\pi}}\int_{-\infty}^{\infty}dx\int_0^1 dz\, e^{ikx}\cos(n\pi z)G(x,z,\tau), \tag{3.3}$$

the transformed solution is readily computed,

$$\hat{G}_n(k,\tau)=\sqrt{\frac{2}{\pi}}\cos(n\pi Z_0)e^{ikX_0-\tau(n^2\pi^2+k^2)}. \tag{3.4}$$

Therefore, the Green's function in the physical domain as a cosine series is [5]

$$\begin{aligned} G(x,z,\tau)=G(x,z,\tau;X_0,Z_0)&=\frac{e^{-\frac{(x-X_0)^2}{4\tau}}}{\sqrt{\pi\tau}}\left[\frac{1}{2}+\sum_{n=1}^{\infty}\cos(n\pi z)\cos(n\pi Z_0)e^{-n^2\pi^2\tau}\right] \\ &=\frac{e^{-\frac{(x-X_0)^2}{4\tau}}}{4\pi\tau}\sum_{n=-\infty}^{\infty}\left[e^{-\frac{(z-Z_0+2n)^2}{4\tau}}+e^{-\frac{(z+Z_0+2n)^2}{4\tau}}\right], \end{aligned} \tag{3.5}$$

with the alternative form as a sum of exponentials that can be derived by the method of images. Essentially this is just the product of the solution to the 1D problem with decay at infinity on the real line, $G_u(x,\tau;X_0)=e^{-\frac{(x-X_0)^2}{4\tau}}/\sqrt{4\pi\tau}$, and that with Neumann boundary conditions in the closed interval $[0,1]$,

$$\begin{aligned} G_b(z,\tau;Z_0)&=1+2\sum_{n=1}^{\infty}\cos(n\pi z)\cos(n\pi Z_0)e^{-n^2\pi^2\tau} \\ &=\frac{1}{\sqrt{4\pi\tau}}\sum_{n=-\infty}^{\infty}\left[e^{-\frac{(z-Z_0+2n)^2}{4\tau}}+e^{-\frac{(z+Z_0+2n)^2}{4\tau}}\right]. \end{aligned} \tag{3.6}$$

3.2. Stochastic ODE for channel flow and the calculation of scalar variance for delta Function initial data. With the Green's function defined, next we compute the scalar variance for the case of channel flow. Here, we derive the general solution for an initial condition which is a delta function in the longitudinal direction, and a delta function located at height Z_0 in the transverse direction. This general formula eventually limits in long time to the exact effective diffusivity computed by multi-scale averaging in the previous section.

The problem of a diffusing passive scalar advected by a longitudinal, parabolic shear in the same channel has the following nondimensionalized SDE representation

$$\begin{cases} dX = 4\,\mathrm{Pe}\left[Z(1-Z)-\frac{1}{6}\right]d\tau+\sqrt{2}\,dW_1, \\ dZ = \sqrt{2}\,dW_2, \end{cases} \tag{3.7}$$

with the Péclet number Pe defined previously in (2.6) and $W_1(\tau)$ is the 1D, free-space Brownian motion whereas $W_2(\tau)$ is the 1D Brownian motion with reflective, solid wall boundaries at $z=0,1$. The solution to this SDE is

$$\begin{cases} X(\tau) = X_0+\frac{2}{3}\,\mathrm{Pe}\,\tau+4\mathrm{Pe}\int_0^\tau Z(s)[1-Z(s)]ds+\sqrt{2}\,W_1(\tau), \\ Z(\tau) = Z_0+\sqrt{2}\,W_2(\tau), \end{cases} \tag{3.8}$$

where (X_0,Z_0) is the starting location of a scalar particle at $t=0$. Consequently, the variance of a scalar particle's displacement along each direction is

$$\begin{aligned} \left\langle X^2(\tau)\right\rangle_\omega-\left\langle X(\tau)\right\rangle_\omega^2 &= 2\tau+16\mathrm{Pe}^2\Big\langle\int_0^\tau\int_0^\tau Z(s)Z(s')[1-Z(s)][1-Z(s')]dsds'\Big\rangle_\omega \\ &\quad -16\mathrm{Pe}^2\Big\{\int_0^\tau\left\langle Z(s)[1-Z(s)]\right\rangle_\omega ds\Big\}^2, \\ \left\langle Z^2(\tau)\right\rangle_\omega-\left\langle Z(\tau)\right\rangle_\omega^2 &= 2\left\langle W_2^2(\tau)\right\rangle_\omega. \end{aligned} \tag{3.9}$$

It should be clear that this formulation indeed applies to arbitrary longitudinal flow $V(z)$, which replaces $4\,\mathrm{Pe}[Z(1-Z)-1/6]$ above, and it applies to other boundary conditions which correspond to Brownian motions subject to different geometries other than a channel specified earlier.

The significant statistical properties of bounded Brownian motion to reduce (3.9) to explicit, closed-form formulas are 1) the variance of the bounded Brownian motion starting at $z=Z_0$, and 2) the temporal correlations of the bounded Brownian motion starting at $z=Z_0$ emerging from the integrals that contribute to $\left\langle X^2(\tau)\right\rangle_\omega-\left\langle X(\tau)\right\rangle_\omega^2$: $\left\langle Z(s)Z(s')\right\rangle_\omega$, $\left\langle Z^2(s)Z(s')\right\rangle_\omega$, $\left\langle Z^2(s)Z^2(s')\right\rangle_\omega$, and their integrals in the temporal box $[0,\tau]^2$.

Unfortunately, the bounded nature of W_2, whose statistics depends on the starting position Z_0, prevents rescaling these processes to random variables in time, which in contrast applies to classical Brownian motions in free space and thus simplifies the calculations greatly. The variance of bounded Brownian motion is relatively easy to compute with the knowledge of (3.6), namely,

$$\begin{aligned} \left\langle Z^2(\tau)\right\rangle_\omega-\left\langle Z(\tau)\right\rangle_\omega^2 &= \int_0^1(z-Z_0)^2G_b(z,\tau;Z_0)dz \\ &= \frac{1-3Z_0+3Z_0^2}{3}+4\sum_{n=1}^\infty\frac{(-1)^n(1-Z_0)+Z_0}{\pi^2n^2}\cos(n\pi Z_0)e^{-n^2\pi^2\tau}. \end{aligned} \tag{3.10}$$

However, the temporal correlations of the Brownian motion in the bounded z-direction that starts at Z_0, $Z(t)$, are more complicated since we need to know the joint probability density $f_{Z(s),Z(\tau)}(y,x)$. Here we resort to conditional probabilities to chain the paths together, $f_{Z(s'),Z(s)}(y,x)=f_{Z(s')|Z(s)}(y|x)\times f_{Z(s)}(x)$ assuming $s'>s$, since the conditional probability, $f_{Z(s')|Z(s)}(y|x)=G_b(y,x,s'-s)$, and the marginal probability, $f_{Z(s)}(x)=G_b(x,Z_0,s)$, are readily available from the Green's function (3.5) due to

the Markovian nature of Brownian motion. Then the temporal correlation can be computed as

$$\begin{aligned}\big\langle Z^m(s)Z^n(s')\big\rangle_\omega &= \int_{[0,1]^2} x^m y^n f_{Z(s),Z(s')}(x,y)dxdy \\ &= \int_{[0,1]^2} x^m y^n G_b(y,x,s'-s)G_b(x,Z_0,s)dxdy. \end{aligned} \tag{3.11}$$

Taking the symmetries in the integration domain and in the integrand into account, we have

$$\begin{aligned}&\int_{[0,\tau]^2} \big\langle Z(s)Z(s')\big\rangle_\omega ds\,ds' \\ &= 8\int_0^\tau ds' \int_0^{s'} ds \int_{[0,1]^2} \Big\{ xy\big[\frac{1}{2}+\sum_{n=1}^\infty \cos(n\pi x)\cos(n\pi Z_0)e^{-n^2\pi^2 s}\big] \\ &\quad \times\big[\frac{1}{2}+\sum_{m=1}^\infty \cos(m\pi y)\cos(m\pi x)e^{-m^2\pi^2(s'-s)}\big]\Big\}dxdy \\ &= I_{11}+I_{12}+I_{13}, \end{aligned} \tag{3.12}$$

where

$$\begin{aligned} I_{11} &= \int_0^\tau ds' \int_0^{s'} ds \int_0^1 dx\big[x+4x\sum_{m=1}^\infty \frac{(-1)^m-1}{m^2\pi^2}\cos(m\pi x)e^{-m^2\pi^2(s'-s)}\big] \\ &= \frac{\tau^2}{4}+\frac{4}{\pi^8}\sum_{m=1}^\infty \frac{[(-1)^m-1]^2}{m^8}\big[m^2\pi^2\tau+(e^{-m^2\pi^2\tau}-1)\big], \end{aligned} \tag{3.13}$$

$$\begin{aligned} I_{12} &= \int_0^\tau ds' \int_0^{s'} ds \int_0^1 dx\Big[2x\sum_{m=1}^\infty \cos(m\pi x)\cos(m\pi Z_0)e^{-m^2\pi^2 s}\Big] \\ &= \frac{2}{\pi^6}\sum_{m=1}^\infty \frac{(-1)^m-1}{m^6}\cos(m\pi Z_0)\big[m^2\pi^2\tau+(e^{-m^2\pi^2\tau}-1)\big], \end{aligned} \tag{3.14}$$

$$\begin{aligned} I_{13} &= 8\sum_{m,n=1}^\infty \frac{(-1)^m-1}{m^2\pi^2}\cos(n\pi Z_0)\int_0^\tau ds' \int_0^{s'} ds \int_0^1 dx\Big\{x\cos(m\pi x) \\ &\quad \times\cos(n\pi x)e^{-m^2\pi^2(s'-s)-n^2\pi^2 s}\Big\} \\ &= \frac{8}{\pi^8}\sum_{m,n=1,\,m\neq n}^\infty \frac{[(-1)^m-1][(-1)^{m-n}-1](m^2+n^2)}{m^4n^2(m^2-n^2)^3}\cos(n\pi Z_0) \\ &\quad \times\Big[m^2(1-e^{-n^2\pi^2\tau})+n^2(e^{-m^2\pi^2\tau}-1)\Big] \\ &\quad +\frac{2}{\pi^6}\sum_{n=1}^\infty \cos(n\pi Z_0)\frac{[(-1)^n-1][1-e^{-n^2\pi^2\tau}(1+n^2\pi^2\tau)]}{n^6}. \end{aligned} \tag{3.15}$$

Similarly,

$$\begin{aligned}\int_{[0,\tau]^2}\big\langle Z^2(s)Z^2(s')\big\rangle_\omega dsds' &= 8\int_0^\tau d\tau\int_0^{s'} ds\int_{[0,1]^2}\Big\{x^2y^2\\ &\quad\times\Big[\frac{1}{2}+\sum_{n=1}^{\infty}\cos(n\pi x)\cos(n\pi Z_0)e^{-n^2\pi^2 s}\Big]\\ &\quad\times\Big[\frac{1}{2}+\sum_{m=1}^{\infty}\cos(m\pi a)\cos(m\pi x)e^{-m^2\pi^2(s'-s)}\Big]\Big\}dxdy\\ &= I_{21}+I_{22}+I_{23},\end{aligned}\tag{3.16}$$

and

$$\begin{aligned}\int_{[0,\tau]^2}\big\langle Z^2(s)Z(s')\big\rangle_\omega dsds' &= 4\int_0^\tau ds'\int_0^{s'} ds\int_{[0,1]^2}\Big\{(x^2y+xy^2)\\ &\quad\times\Big[\frac{1}{2}+\sum_{n=1}^{\infty}\cos(n\pi x)\cos(n\pi Z_0)e^{-n^2\pi^2 s}\Big]\\ &\quad\times\Big[\frac{1}{2}+\sum_{m=1}^{\infty}\cos(m\pi y)\cos(m\pi x)e^{-m^2\pi^2(s'-s)}\Big]\Big\}dxdy\\ &= I_{31}+I_{32}+I_{33}+I_{34}+I_{35}+I_{36},\end{aligned}\tag{3.17}$$

for which the explicit calculations of I_{21} through I_{23} and I_{31} through I_{36} are tedious but very similar to those of I_{11}, I_{12} and I_{13} as shown in (3.13) through (3.15). The details of computing these averages can be found in Appendix.

Substituting the results from (3.12) through (3.16) into (3.9) and with the similar but tedious calculations for $\big\langle X(\tau)\big\rangle_\omega^2$, we arrive at

$$\begin{aligned}\big\langle X^2(\tau)\big\rangle_\omega &= X_0^2+2\tau+\frac{4\mathrm{Pe}^2}{\pi^6}\sum_{n=1}^{\infty}\frac{1}{n^6}\big[\tau+\frac{e^{-4n^2\pi^2\tau}-1}{4n^2\pi^2}\big]\\ &\quad-\frac{4\mathrm{Pe}^2}{3\pi^4}\sum_{n=1}^{\infty}\frac{\cos(2n\pi Z_0)}{n^4}\big[\tau+\frac{e^{-4n^2\pi^2\tau}-1}{4n^2\pi^2}\big]+\frac{2\mathrm{Pe}^2}{\pi^6}\sum_{m,n=1}^{\infty}\cos(2n\pi Z_0)K_{mn}(\tau),\\ \big\langle X(\tau)\big\rangle_\omega^2 &= X_0^2-\frac{4\mathrm{Pe}^2}{3\pi^4}\sum_{n=1}^{\infty}\frac{\cos(2n\pi Z_0)}{n^4}(\tau-\tau e^{-4n^2\pi^2\tau})\\ &\quad+\frac{\mathrm{Pe}^2}{\pi^8}\big[\sum_{n=1}^{\infty}\frac{\cos(2n\pi Z_0)(e^{-4n^2\pi^2\tau}-1)}{n^4}\big]^2,\end{aligned}\tag{3.18}$$

with

$$K_{mn}(\tau)=\begin{cases}\dfrac{m^2+n^2}{\pi^2m^2(m^2-n^2)^3}\Big[\frac{1-e^{-4n^2\pi^2\tau}}{n^2}+\frac{e^{-4m^2\pi^2\tau}-1}{m^2}\Big], & m\neq n,\\ \dfrac{1}{2n^6}\Big[\dfrac{1}{4n^2\pi^2}-\dfrac{1}{3}\Big]\Big[1-e^{-4n^2\pi^2\tau}(1+4n^2\pi^2\tau)\Big], & m=n.\end{cases}\tag{3.19}$$

Consequently, we define the diffusivity enhancement via the exact longitudinal flow-enhanced variance compared to the pure diffusion variance, 2τ, of a particle that starts at an arbitrary location (X_0, Z_0) at an arbitrary time as

$$\begin{aligned}\frac{\kappa_{eff}}{\kappa} &\equiv \frac{\left\langle X^2(\tau)\right\rangle_\omega - \left\langle X(\tau)\right\rangle_\omega^2}{2\tau} \\ &= 1 + \frac{2\mathrm{Pe}^2}{\pi^6}\sum_{n=1}^{\infty}\frac{1}{n^6}\left[1 + \frac{e^{-4n^2\pi^2\tau}-1}{4n^2\pi^2\tau}\right] \\ &\quad - \frac{2\mathrm{Pe}^2}{3\pi^4}\sum_{n=1}^{\infty}\frac{\cos(2n\pi Z_0)}{n^4}\left[e^{-4n^2\pi^2\tau} + \frac{e^{-4n^2\pi^2\tau}-1}{4n^2\pi^2\tau}\right] \\ &\quad + \frac{\mathrm{Pe}^2}{\pi^6\tau}\sum_{m,n=1}^{\infty}\cos(2n\pi Z_0)K_{mn}(\tau) - \frac{\mathrm{Pe}^2}{2\pi^8\tau}\left[\sum_{n=1}^{\infty}\frac{\cos(2n\pi Z_0)(e^{-4n^2\pi^2\tau}-1)}{n^4}\right]^2.\end{aligned} \tag{3.20}$$

This result and the analogous formula for the pipe geometry actually solves the first of the partial differential equations in a hierachy of previously established moment equations [1, 5, 6]. However, solving the full hierarchy of those PDEs directly for arbitrary τ and Z_0 is generally impossible even for this simple flow, except for some special cases of initial distributions, and therefore (3.20) were not derived by the moment problem approach. Alternatively, motivated by the relationship between particle displacement and the solution to the diffusion equation, this formula could be obtained by making a Gaussian approximation to the solution to the advection-diffusion equation (2.1) whose variance is expanded in Hermite polynomials [17]. Nonetheless, the Gaussian-Hermite approximation approach is fairly involved and seems hard to generalize compared to the more transparent SDE-based approach presented here.

As $\tau \to \infty$, it is straightforward to see from (3.20) that the long time behavior of the flow-enhanced longitudinal diffusion is

$$\frac{\kappa_{eff}}{\kappa} \sim 1 + \frac{2\mathrm{Pe}^2}{\pi^6}\sum_{m=1}^{\infty}\frac{1}{m^6} = 1 + \frac{2\mathrm{Pe}^2}{945} \tag{3.21}$$

for $\tau \gg 1$, or equivalently $t \gg \frac{a^2}{\kappa}$ in dimensional units. This scaling law (3.21) is exactly the result we obtained in (2.18), for an arbitrary initial scalar distribution.

Next, we will see how the initial transverse distribution of the data establishes a short-time, anomalous regime of the diffusion enhancement, in which $\frac{\kappa_{eff}}{\kappa} \sim 1 + c\mathrm{Pe}^2\tau^\alpha$ with $\alpha = 1$, 2, or 3 depending on different initial data.

3.3. Transversely uniform initial data. The general variance formula just computed enjoys a tremendous simplification when the initial condition is spanwise uniform. This simplification allows for a complete asymptotic expansion for both short and long times, which we show sets the anomalous timescales and scaling exponents rigorously.

For the PDE representation of (3.7), if the initial data consisted of only vertical layers, namely, $T_0(x,z) \equiv \bar{T}_0(x)$, the initial transverse location of a scalar particle, Z_0, can considered as a random variable uniformly distributed in $[0,1]$. Consequently, we

can greatly simplify (3.20) by averaging over $Z_0 \in [0,1]$ to have

$$\frac{\kappa_{eff}}{\kappa} = \frac{\langle X^2(\tau)\rangle_{\omega,Z_0} - \langle X(\tau)\rangle^2_{\omega,Z_0}}{2\tau} = \frac{\int_0^1 \langle X^2(\tau)\rangle_\omega dZ_0 - \left[\int_0^1 \langle X(\tau)\rangle_\omega dZ_0\right]^2}{2\tau}$$

$$= 1 + \frac{2\mathrm{Pe}^2}{\pi^6}\sum_{n=1}^{\infty}\frac{1}{n^6}\left[1 + \frac{e^{-4n^2\pi^2\tau}-1}{4n^2\pi^2\tau}\right] = 1 + \frac{2\mathrm{Pe}^2}{945}\left[1 - \frac{1}{40\tau}\left(1 - \frac{9450}{\pi^8}\sum_{m=1}^{\infty}\frac{e^{-4m^2\pi^2\tau}}{m^8}\right)\right] \tag{3.22}$$

since all the terms with the factor $\cos(n\pi Z_0)$ would be averaged to zero by $\int_0^1 \cos(2n\pi Z_0)dZ_0 = 0, n = 1,2,\ldots$. Generally for a separable initial distribution $T_0(x,z) \equiv X(x)Z(z)$ one has to evaluate integrals $\int_0^a Z(z)\cos(2n\pi z)dz, n = 1,2,\ldots$ to determine the universal diffusion enhancement.

Since

$$\frac{d^4}{da^4}\frac{e^{-am^2}}{m^8} = e^{-am^2}, \qquad \sum_{m=1}^{\infty} e^{-am^2} \sim \sqrt{\frac{\pi}{4a}}, a \to 0 \tag{3.23}$$

and we know that the series in (3.22) is convergent for $\tau \geq 0$, anti-differentiating(3.23) term-by-term and matching the coefficients yields the short-time asymptotics with a *fractional power correction*

$$\frac{\kappa_{eff}}{\kappa} \sim 1 + \frac{16\mathrm{Pe}^2}{3}\left(\frac{\tau}{120} - \frac{\tau^2}{6} + \frac{32\tau^{\frac{5}{2}}}{35\sqrt{\pi}}\right), \qquad \tau \to 0. \tag{3.24}$$

Formulas (3.22) and (3.24) are in agreement with previous results for this special case of initial data [6, 19].

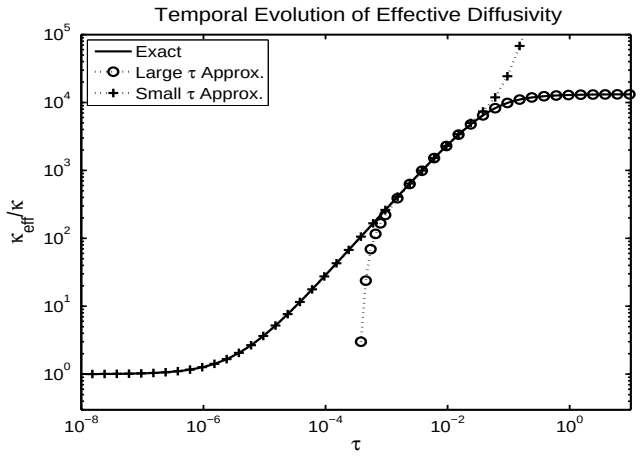

Fig. 3.1: $\frac{\kappa_{eff}}{\kappa}$ vs τ when $\mathrm{Pe} = 2500$ in a rectangular channel with $T_0(x,z) \equiv T_0(x)$.

Figure 3.1 is a log-log plot of the temporal evolution of the non-dimensionalized effective diffusivity (3.22) along with its asymptotic approximations. Here the solid line is the numerical evaluation of (3.22) truncated to 100 terms in the sum, whereas

the large τ approximation only keeps the first two terms and the small τ approximation utilizes (3.24). From the figure, the constant behavior of the diffusion enhancement as $\tau \to 0$ ($\frac{\kappa_{eff}}{\kappa} \approx 1$) and as $\tau \to \infty$ ($\frac{\kappa_{eff}}{\kappa} \approx 1 + \frac{2\mathrm{Pe}^2}{945} \approx 1.32 \times 10^4$), and the linear scaling for intermediate times are evident. Furthermore, the time scale of the first transition from molecular diffusion of the scalar without flow enhancement to an "anomalous" regime is $\tau^* \approx \frac{360}{16}\mathrm{Pe}^{-2} = 3.6 \times 10^{-6}$, just as predicted by the first correction term in (3.24), or in dimensional units, $t \approx \frac{360\kappa}{16U^2}$; whereas when $\tau \approx \frac{1}{4\pi^2} \approx 0.025$, or in dimensional units, $t \approx \frac{a^2}{4\pi^2\kappa}$, the enhancement starts to converge to its long time, constant value $1 + \frac{2\mathrm{Pe}^2}{945}$.

3.4. Point source initial data. The situation is quite different when the initial condition is transversely a delta function located at $Z_0 = b$. The general formula for the scalar variance involves a double series as opposed to a single series, and the complete evaluation of the short time asymptotic expansion (which provides the anomalous timescale) is tedious. Below, we present a study of this behavior and document by numerical summation of the series that the anomalous timescale and scaling exponent is substantially different from the uniform case here, and depends upon the release position $Z_0 = b$. We also demonstrate that the numerical summation accurately agrees with direct Monte-Carlo simulations, and further demonstrate the free space formalism of Latini and Bernoff [8] does accurately capture the anomalous short timescale provided the release position is bounded away from the channel walls. Lastly, we rigorously prove that the anomalous timescale for this case involving transverse point source initial data has order of $O(\mathrm{Pe}^{-1})$ (centerline release), or of $O(\mathrm{Pe}^{-2/3})$ (off-center release), as opposed to the much smaller $O(\mathrm{Pe}^{-2})$ for the uniform case.

Consider the situation when all the particles start at a fixed location within the pipe, $Z_0 = b, b \in (0,1)$, or equivalently, $T_0(x,z) = \bar{T}_0(x)\delta(z-b)$. Although (3.21) holds for the Taylor regime, the time scale of the transition into the short-time, anomalous regime, τ^*, is different and it increases from $O(\mathrm{Pe}^{-2})$ to $O(\mathrm{Pe}^{-\frac{2}{3}})$ if $b = \frac{a}{2}$ ($t \propto \frac{a^{4/3}}{U^{2/3}\kappa^{1/3}}$ in dimensional units), or to $O(\mathrm{Pe}^{-1})$ if $b \neq \frac{1}{2}$ ($t \propto \frac{U}{a}$ in dimensional units) when Pe is large. We stress that this assertion at present hinges upon a numerical summation of the double series representation formula for the scalar variance, unless otherwise noted, the double series is approximated with 50^2 terms and does not show substantial change with the inclusion of more terms. Furthermore, as we will derive below in section 4, using an approximated Gaussian kernel in the calcuations of $\langle\cdot\rangle_\omega$, we directly obtain that the short-time behavior of the enhancement with a point source discharge is

$$\frac{\kappa_{eff}}{\kappa} \sim 1 + \frac{64\left(b - \frac{1}{2}\right)^2 \mathrm{Pe}^2\tau^2}{3} + \frac{32\mathrm{Pe}^2\tau^3}{3}, \qquad \tau \to 0,\ Z_0 = b. \tag{3.25}$$

We can identify two anomalous time scales for point source release at different locations in the channel. Physically, in the case of $T_0(x,z) = \bar{T}_0(x)\delta(z - \frac{1}{2})$, when τ is negligible compared to the molecular diffusion time scale all scalar particles are still close to their initial center-line position, where there is almost no transverse variation in the parabolic shear. Therefore molecular diffusion initially dominates in an almost Galilean translation. However, in the off-center case, $b \neq \frac{a}{2}$, the particles experience the shear and the consequent flow-enhanced diffusion much sooner. Figure 3.2 illustrates the difference in the short time behavior of $\frac{\kappa_{\mathrm{eff}}}{\kappa}$ with two types of initial data. It is clear that the first transition occurs at $\tau^* = O(\mathrm{Pe}^{-1}) \approx 3 \times 10^{-4}$ when $b = \frac{1}{4}$ and at $\tau^* = O(\mathrm{Pe}^{-\frac{2}{3}}) \approx 2.5 \times 10^{-3}$ when $b = \frac{1}{2}$.

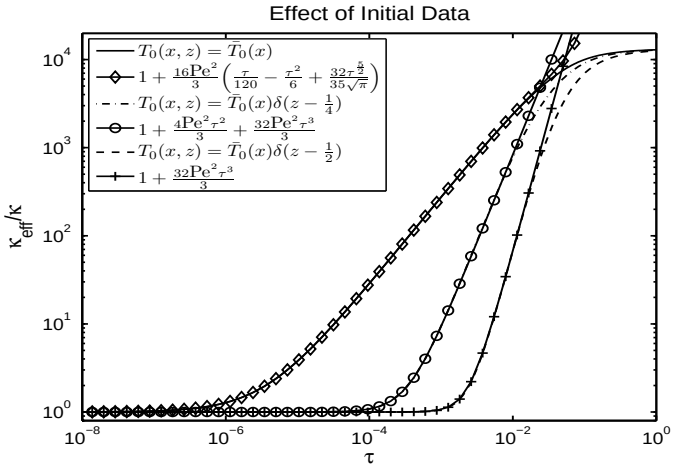

Fig. 3.2: Comparison in $\frac{\kappa_{\mathrm{eff}}}{\kappa}$ between $T_0(x,z)=\bar{T}_0(x)\delta(z-b)$ and $T_0(x,z)=\bar{T}_0(x)$ when $\mathrm{Pe}=2500$.

It should be noted that since the asymptotic estimate (3.25) is obtained from a free-space Gaussian approximation of the exact Brownian kernel G_b, we expect that as Z_0 approaches one of the walls the estimate should start to fail due to the boundary effect. Figure 3.3 lists a sequence of plots for $Z_0\to 0$; the deviation of the estimate (3.25) from the exact value is obvious with decreasing Z_0, although the free-space estimate still accurately captures the time scale of transition into the anomalous regime.

The existence of the alternative time scale, different than $O(\mathrm{Pe}^{-2})$, of the onset of the anomalous regime with point-source discharge can be determined through general short time asymptotic estimates of the exact variance given in equation(3.20). From this equation we can derive a three-term asympotic expansion for $\kappa_{\mathrm{eff}}/\kappa$ as $\tau\to 0$, by expanding the exponentials around $\tau=0$

$$\frac{\kappa_{eff}}{\kappa}\sim 1+\frac{8\mathrm{Pe}^2\tau}{\pi^4}\Big[\sum_{m=1}^{\infty}\frac{4+\cos(2m\pi Z_0)}{8m^4}-\Big(\sum_{m=1}^{\infty}\frac{\cos(2m\pi Z_0)}{m^2}\Big)^2 + \sum_{\substack{m,n=1,\\ m\neq n}}^{\infty}\frac{\cos(2n\pi Z_0)(n^2+m^2)}{m^2(n^2-m^2)^2}\Big]+C_2\mathrm{Pe}^2\tau^2+o(\mathrm{Pe}^2\tau^2),\qquad \tau\to 0. \tag{3.26}$$

Rigorously showing hat this expansion is asymptotic is complicated by several factors. First, observe that several of the series in equation (3.20) involve division by τ. Second, although all the series involved and their term by term derivatives converge absolutely for $\tau>0$, it is not immediately obvious that this differentiation property extends to $\tau=0$. To demonstrate that this approximation is asymptotic, we will next show that $\kappa_{\mathrm{eff}}/\kappa\sim 1+o(\tau)$ as $\tau\to 0$, and leave proving the next expansion term to future work (here, we present this last term only formally). To this end, we re-write the enhanced diffusion in equation (3.20) grouping terms which form the coefficient of the factor

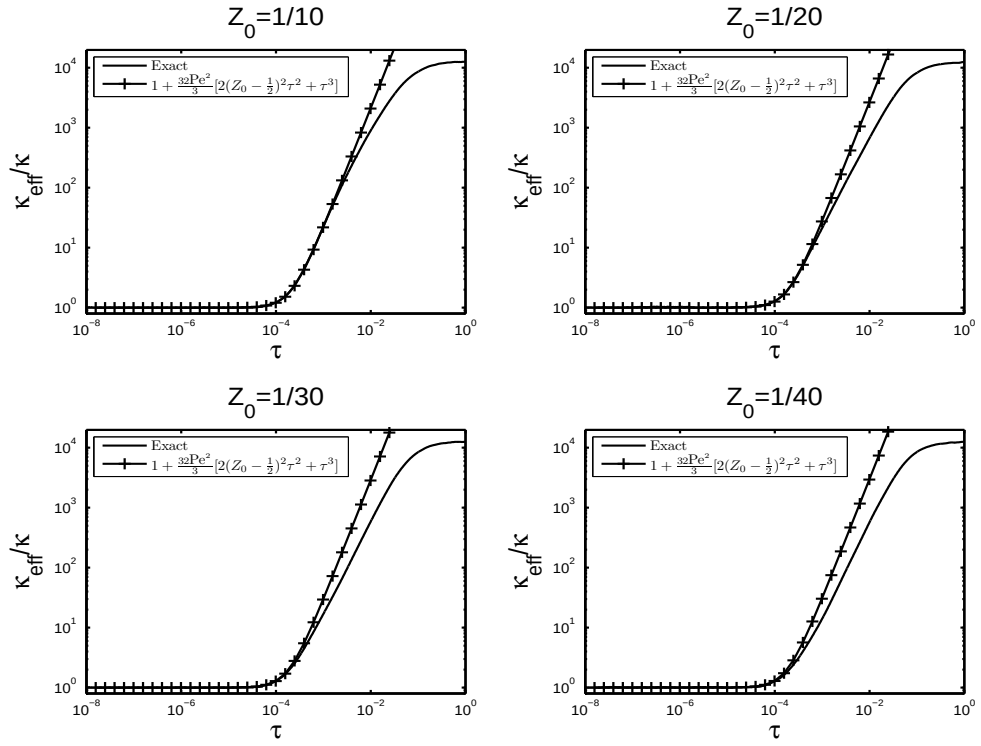

Fig. 3.3: Asymptotics of $\frac{\kappa_{\text{eff}}}{\kappa}$ with $T_0(x,z)=\bar{T}_0(x)\delta(z-b)$ when $\text{Pe}=2500$.

$1/\tau$ as $\mathcal{G}(\tau)$ and the rest as $\mathcal{F}(\tau)$:

$$\frac{\kappa_{\text{eff}}}{\kappa}=\mathcal{F}(\tau)+\frac{\mathcal{G}(\tau)}{\tau}.$$

It may be directly shown that $\mathcal{G}(\tau)$ is twice continuously differentiable for all $Z_0\in[0,1]$, $\tau\geq 0$, and the third derivative exists for all $\tau>0$, since term-wise differentiation yields absolutely convergent series for two derivatives, and the third derivative is absolutely convergent for $\tau>0$ thanks to the rapidly decaying exponentials in the sum indices. By utilizing Taylor's theorem with remainder, this allows us to write

$$\mathcal{G}(\tau)=\tau\mathcal{G}'(0)+\frac{\tau^2}{2}\mathcal{G}''(0)+\frac{\tau^3}{6}\mathcal{G}'''(\tau_1^*),\qquad \mathcal{F}(\tau)=\mathcal{F}(0)+\tau\mathcal{F}'(0)+\frac{\tau^2}{2}\mathcal{F}''(\tau_2^*).$$

Inspection of the series involved shows that $\mathcal{G}(0)=0$ and $\mathcal{G}'(0)+\mathcal{F}(0)=1$. Further, since $\tau_{1,2}^*>0$ this leads to

$$\frac{\kappa_{\text{eff}}}{\kappa}=1+\tau(\mathcal{F}'(0)+\frac{1}{2}\mathcal{G}''(0))+o(\tau).$$

The following calculations explicitly show the linear coefficient is zero, and further formally compute the quadratic coefficient hidden in $o(\tau)$ as well as establish the convergence of the double sum of positive numbers,

$$\sum_{n=1,n\neq m}^{\infty}\frac{(n^2+m^2)}{m^2(n^2-m^2)^2},$$

which arises from the second derivative of $K_{mn}(\tau)$ at $\tau=0$. Using the identities involving polylogarithm $\mathrm{Li}_n(z)$ and Bernoulli polynomials $B_n(z)$ [2]

$$\sum_{m=1}^{\infty}\frac{\cos(2m\pi Z_0)}{m^2}=\frac{\mathrm{Li}_2(e^{2\pi iZ_0})+\mathrm{Li}_2(e^{-2\pi iZ_0})}{2}=\pi^2B_2(Z_0)=\pi^2\Big(Z_0^2-Z_0+\frac{1}{6}\Big) \quad (3.27)$$

and noticing that

$$\sum_{n=1}^{\infty}\frac{\cos(2n\pi Z_0)(n^2+x^2)}{(n^2-x^2)^2}=\frac{1}{2}\Big[\frac{\pi^2\cos(2\pi Z_0x)}{\sin^2(\pi x)}-\frac{1}{x^2}\Big],\quad x\neq 1,2,\ldots, \quad (3.28)$$

yields

$$\begin{aligned}\sum_{\substack{n=1,\\ n\neq m}}^{\infty}\frac{\cos(2n\pi Z_0)(n^2+m^2)}{(n^2-m^2)^2}&=\lim_{x\to m}\Big(\frac{\pi^2\cos(2\pi Z_0x)}{2\sin^2(\pi x)}-\frac{1}{2x^2}-\frac{\cos(2m\pi Z_0)(m^2+x^2)}{(m^2-x^2)^2}\Big)\\ &=\cos(2m\pi Z_0)\Big[\pi^2\Big(Z_0^2-Z_0+\frac{1}{6}\Big)-\frac{1}{8m^2}\Big]-\frac{1}{2m^2}\end{aligned} \quad (3.29)$$

for $m=1,2,\ldots$ and finally

$$\sum_{\substack{m,n=1,\\ m\neq n}}^{\infty}\frac{\cos(2n\pi Z_0)(n^2+m^2)}{m^2(n^2-m^2)^2}=\Big(\sum_{m=1}^{\infty}\frac{\cos(2m\pi Z_0)}{m^2}\Big)^2-\sum_{m=1}^{\infty}\frac{4+\cos(2m\pi Z_0)}{8m^4}. \quad (3.30)$$

Thus the linear term of τ in the expansion (3.26) vanishes

$$\frac{\kappa_{\mathit{eff}}}{\kappa}\sim 1+C_2\mathrm{Pe}^2\tau^2+o(\mathrm{Pe}^2\tau^2),\qquad \tau\to 0,\ \forall Z_0\in[0,1], \quad (3.31)$$

which implies that the onset of the anomalous regime is at least $O(\mathrm{Pe}^{-1})$ for $\mathrm{Pe}\gg 1$, instead of $O(\mathrm{Pe}^{-2})$ as in the case with uniform transverse data. A very similar, but more involved calculation shows explicitly a non-zero, quadratic correction in (3.26)

$$C_2\mathrm{Pe}^2\tau^2=\frac{64\mathrm{Pe}^2}{3}B_1^2(Z_0)\,\tau^2=\frac{64\mathrm{Pe}^2}{3}\Big(Z_0-\frac{1}{2}\Big)^2\tau^2. \quad (3.32)$$

For higher order corrections, straightforward Taylor expansion leads to divergent series and further analysis is required.

4. The circular pipe

In this section we consider the case of circular pipe flow. The behavior is quite similar to channel flow, provided we focus upon axisymmetric initial scalar distributions: essentially all of the results for channel flow extend to pipe flow, though the rigorous computation of the long time limit exactly connecting to the multi-scale effective diffusivity requires some special identities borrowed from the quantum mechanics community.

Assuming axisymmetric initial data, the SDE calculations in a pipe geometry are very similar to the channel case demonstrated before, but the Brownian kernel with reflective boundaries in the transverse direction now becomes [5]

$$G(y,z,\tau;Y_0,Z_0)=G_p(r,\tau;R_0)=\frac{1}{\pi}\Big[1+\sum_{n=1}^{\infty}\frac{J_0(\mu_nr)J_0(\mu_nR_0)}{J_0^2(\mu_n)}\,e^{-\mu_n^2\tau}\Big] \quad (4.1)$$

in cylindrical coordinates $r=\sqrt{y^2+z^2}$ and $R_0=\sqrt{Y_0^2+Z_0^2}$, instead of the heat kernel on a closed interval $[0,1]$, $G_b(z,Z_0,\tau)$. Here $J_\nu(z)$ are the ν^{th}-order Bessel Functions of the first kind and μ_n, $n=1,2,\dots$ solve $J_1(\mu_n)=0$.

4.1. General scalar variance formula for pipe flow. Since the mean-zero, parabolic shear in a pipe is $u(y,z)=u(r)=U(\frac{1}{2}-r^2)$, the mean square displacement along the x-axis is

$$\begin{aligned}\big\langle (X(\tau)-X_0)^2\big\rangle_\omega &= 2\tau+\mathrm{Pe}^2\Big\langle \int_0^\tau\int_0^\tau [\frac{1}{2}-R^2(s)][\frac{1}{2}-R^2(s')]ds\,ds'\Big\rangle_\omega\\ &= 2\tau+\mathrm{Pe}^2\Big(\frac{\tau^2}{4}-\tau\int_0^\tau \big\langle R^2(s)\big\rangle_\omega ds+\int_0^\tau\int_0^\tau \big\langle R^2(s)R^2(s')\big\rangle_\omega ds\,ds'\Big),\end{aligned} \tag{4.2}$$

where $R(t)$ is the radial Brownian motion in the cross-section of the pipe with initial position R_0 and density distribution (4.1). The averages in (4.2) are computed as follows:

$$\begin{aligned}\int_0^\tau \big\langle R^2(s)\big\rangle_\omega ds &= \int_0^\tau\int_0^1 r^2 G_p(r,s;R_0)2\pi r\,dr\,ds\\ &= \frac{1}{2}+2\sum_{n=1}^\infty \frac{J_0(\mu_n R_0)}{J_0^2(\mu_n)}\Big(\int_0^1 r^3 J_0(\mu_n r)dr\Big)\Big(\int_0^t e^{-\mu_n^2 s}ds\Big)\\ &= \frac{\tau}{2}+2\sum_{n=1}^\infty \frac{J_0(\mu_n R_0)[2J_2(\mu_n)-\mu_n J_3(\mu_n)]}{\mu_n^4 J_0^2(\mu_n)}\big(1-e^{-\mu_n^2\tau}\big),\end{aligned} \tag{4.3}$$

$$\begin{aligned}&\int_{[0,\tau]^2}\big\langle R^2(s)R^2(s')\big\rangle_\omega ds\,ds'\\ &=2\int_0^\tau ds'\int_0^{s'} ds\Big\{\int_{[0,1]^2} x^2y^2G_p(y,s'-s;x)G_p(x,s;Z_0)4\pi^2xy\,dx\,dy\Big\}\\ &=\frac{\tau^2}{4}+8\tau\sum_{n=1}^\infty\frac{[2J_2(\mu_n)-\mu_nJ_3(\mu_n)]^2}{\mu_n^8J_0^2(\mu_n)}\Big[\mu_n^2-\frac{1-e^{-\mu_n^2\tau}}{\tau}\Big]\\ &\quad+2\tau\sum_{n=1}^\infty\frac{J_0(\mu_nR_0)[2J_2(\mu_n)-\mu_nJ_3(\mu_n)]}{\mu_n^6J_0^2(\mu_n)}\Big[\mu_n^2-\frac{1-e^{-\mu_n^2\tau}}{\tau}\Big]\\ &\quad+16\sum_{m,n=1}^\infty J_0(\mu_mR_0)\bar K_{mn}(\tau),\end{aligned} \tag{4.4}$$

where

$$\bar K_{mn}(\tau)=\begin{cases}\dfrac{\mu_m^2\big(1-e^{-\mu_n^2\tau}\big)-\mu_n^2\big(1-e^{-\mu_m^2\tau}\big)}{\mu_n^4\mu_m^2(\mu_m^2-\mu_n^2)J_0(\mu_n)J_0^2(\mu_m)}\int_0^1 r^3J_0(\mu_nr)J_0(\mu_mr)dr, & m\neq n,\\ \dfrac{1-e^{-\mu_m^2\tau}\big(1+\mu_m^2\tau\big)}{\mu_m^6J_0^3(\mu_m)}\int_0^1 r^3J_0^2(\mu_mr)dr, & m=n.\end{cases} \tag{4.5}$$

To summarize, the flow-enhanced diffusion is

$$\begin{aligned}\frac{\kappa_{\text{eff}}}{\kappa} &= \frac{\langle X(\tau)^2\rangle_\omega - \langle X(\tau)\rangle_\omega^2}{2\tau} = \frac{\langle [X(\tau)-X_0]^2\rangle_\omega - \langle X(\tau)-X_0\rangle_\omega^2}{2\tau} \\ &= 1+\text{Pe}^2\sum_{n=1}^{\infty}\left\{\frac{16}{\mu_n^6}\Big[1-\frac{\big(1-e^{-\mu_n^2\tau}\big)}{\mu_n^2\tau}\Big]+\frac{2J_0(\mu_n R_0)}{\mu_n^4 J_0(\mu_n)}\Big[e^{-\mu_n^2\tau}-\frac{\big(1-e^{-\mu_n^2\tau}\big)}{\mu_n^2\tau}\Big]\right\} \\ &\quad +\frac{8\text{Pe}^2}{\tau}\left\{\sum_{m,n=1}^{\infty} J_0(\mu_m R_0)\bar{K}_{mn}(\tau)-\Big[\sum_{n=1}^{\infty}\frac{J_0(\mu_n R_0)}{\mu_n^4 J_0(\mu_n)}\big(e^{-\mu_n^2\tau}-1\big)\Big]^2\right\}, \qquad (4.6)\end{aligned}$$

utilizing the recurrence identity $J_{\nu-1}(z)+J_{\nu+1}(z)=\frac{2\nu}{z}J_\nu(z)$, $\nu=1,2,\dots$ [2].

4.2. Transversely uniform initial data in pipe flow. Similar to (3.22), if we further assume that the initial condition is independent of r, the above formula reduces to

$$\frac{\kappa_{\text{eff}}}{\kappa}=1+\frac{\text{Pe}^2}{192}\Big[1-\frac{1}{15\tau}\Big(1-46080\sum_{n=1}^{\infty}\frac{e^{-\mu_n^2\tau}}{\mu_n^8}\Big)\Big] \qquad (4.7)$$

since the averages $\int_0^1 rJ_0(\mu_n r)dr=J_1(\mu_n)=0$, $n=1,2,\dots$ and

$$\xi(2s):=\sum_{n=1}^{\infty}\frac{1}{\mu_n^{2s}}=\frac{1}{s+1}\sum_{n=1}^{s-1}\xi(2n)\,\xi(2s-2n), \qquad s=2,3,\dots \qquad (4.8)$$

with $\xi(2)=\frac{1}{8}$ [7].

As $\tau\to\infty$, we have

$$\frac{\kappa_{\text{eff}}}{\kappa}\to 1+\frac{\text{Pe}^2}{192}, \qquad (4.9)$$

whereas for $\tau\to 0$, with a similar calculation as in the channel case, we recover the formula [6]

$$\frac{\kappa_{\text{eff}}}{\kappa}\sim 1+\text{Pe}^2\Big(\frac{\tau}{24}-\frac{\tau^2}{3}+\frac{128\tau^{\frac{5}{2}}}{105\sqrt{\pi}}\Big). \qquad (4.10)$$

Figure 4.1 illustrates the temporal evolution of the effective diffusivity in a circular pipe described by (4.7), which is very similar as the channel case shown in figure 3.1.

Moreover, similar to the channel case if the initial condition is concentrated at a fixed radius in the pipe, namely, $R_0=b$, the short time behavior of $\frac{\kappa_{\text{eff}}}{\kappa}$ becomes

$$\frac{\kappa_{\text{eff}}}{\kappa}\sim 1+\frac{4b^2\text{Pe}^2\tau^2}{3}+\frac{4\text{Pe}^2\tau^3}{3}, \quad \tau\to 0,\ R_0=b. \qquad (4.11)$$

4.3. Short time approximations with gaussian kernels. The scaling laws (3.24) and (4.10) provide detailed information about the short time behavior of the diffusion enhancement, in terms of the transitional time scale between the initial diffusion regime and the anomalous, ballistic regime when the initial distribution is transversely uniform. However, they were obtained from small τ expansions and summing of the exact formulas (3.20) and (4.6). Such a technique is difficult to apply

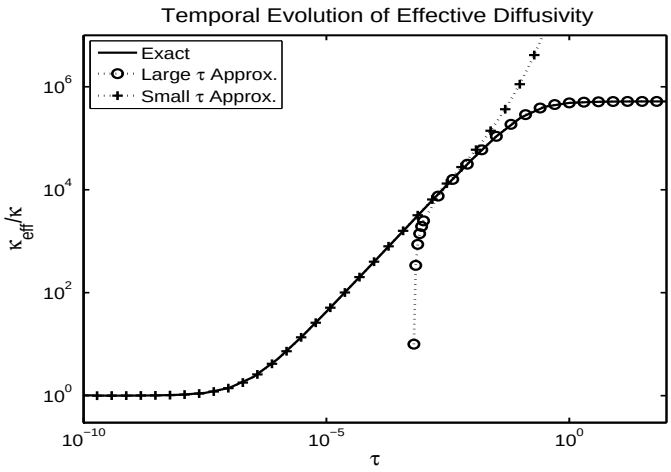

Fig. 4.1: $\frac{\kappa_{eff}}{\kappa}$ vs τ when $\mathrm{Pe}=10^4$, $T_0(r)\equiv$const in a circular pipe.

to the point source discharge when the complete formulas involve series with the terms $\cos(n\pi Z_0)$ or $J_0(\mu_n R_0)$.

Latini and Bernoff [8] demonstrated how to obtain the short-time, transitional scalings for point sources with the exact solution of equation (2.1) with free-space boundary conditions, and this approach required a solution ansatz originally proposed by Lighthill [11]. They were motivated by the physical intuition that for very small times before the molecular diffusion effect is significant, the rigid boundaries do not affect the scalars in the interior of the channel. However, with the same motivation, the SDE approach as we discussed actually yields more complete and general results in a straightforward way, which ultimately leads to the asymptotic relations (3.25) and (4.11).

Assuming that initially the boundary effects are negligible, we can approximate the bounded Brownian kernels G_b and G_p by their free-space counterparts, namely, Gaussians:

$$G_b(z,\tau;Z_0)\approx\frac{e^{-\frac{(z-Z_0)^2}{4\tau}}}{\sqrt{4\pi\tau}},\quad G_p(y,z,\tau;Y_0,Z_0)\approx\frac{e^{-\frac{(y-Y_0)^2+(z-Z_0)^2}{4\tau}}}{4\pi\tau}. \tag{4.12}$$

Essentially, here the bounded Brownian motion $W_2(\tau)$ in (3.8) is approximated by free space Brownian motion $B(\tau)\sim\mathcal{N}(0,\tau)$ on short times.

Now we consider the free space problem as a short-time approximation to the channel problem under an arbitrary steady, smooth shear flow. For any $Z_0\in(0,1)$ around which there exists a neighborhood Ω such that a general shearing flow $u(z)$ has a power series expansion

$$u(z)=\sum_{k=0}^{\infty}\frac{u^{(k)}(Z_0)}{k!}(z-Z_0)^k \tag{4.13}$$

on Ω, the mean square displacement in the sheared x-direction over Ω can then be easily computed by plugging in $z=Z(\tau)=Z_0+B(\tau)$, since the averages over the Brownian motion B are straightforward Gaussian integrals. In particular, given an arbitrary

initial data distribution of Z_0 on Ω with density function $\mu(Z_0)$, averaging over the space of the Brownian paths and over $\mu(Z_0)$ reads

$$\begin{aligned}
&\Big\langle X^2(\tau)\Big\rangle - \Big\langle X(\tau)\Big\rangle^2 \\
&\approx 2\tau + \sum_{j,k=0}^{\infty} a_j a_k \int_0^\tau \int_0^\tau \Big\langle B(t)^j B(s)^k \Big\rangle ds dt - \Big[\sum_{k=0}^{\infty} a_k \int_0^\tau \Big\langle B(s)^k \Big\rangle ds\Big]^2 \\
&\approx 2\tau + \tau^2\Big(\overline{a_0^2} - \overline{a_0}^2\Big) + 2\tau^3\Big(\frac{1}{3}\overline{a_1^2} + \overline{a_0 a_2} - \overline{a_0}\,\overline{a_2}\Big) \\
&\quad + \tau^4\Big(\frac{7}{3}\overline{a_2^2} - \overline{a_2}^2 + 2\overline{a_0 a_3} - 2\overline{a_0}\,\overline{a_3}\Big) + O(\tau^5)
\end{aligned} \tag{4.14}$$

in which

$$\overline{f(Z_0)} = \int_\Omega f(Z_0)\mu(Z_0) dZ_0 \tag{4.15}$$

is the average taken over the initial distribution $\mu(Z_0)$. In the special case of quadratic shear $u(Z) = 4\mathrm{Pe}\, Z(1-Z)$,

$$a_0 = 4\mathrm{Pe}\, Z_0(1-Z_0),\ a_1 = 4\mathrm{Pe}(1-2Z_0),\ a_2 = -4\mathrm{Pe},\ a_3 = a_4 = \cdots = 0. \tag{4.16}$$

Clearly, for a general distribution μ the coefficients of different powers of τ in (4.14) do not vanish. But when $\mu(Z_0)$ is a Dirac delta, the coefficient of the τ^2, and more generally, the difference $\overline{a_i a_j} - \overline{a_i}\,\overline{a_j}$, $i,j = 0,1,2,\ldots$, vanishes. This establishes for a general class of (smooth) shear flows that, generically, the short time variance expansion (4.14) will have a non-zero quadratic (in time) correction unless the initial distribution is a Dirac delta in the transverse direction.

Furthermore, if $\mu(Z_0) = \delta(Z_0 - 1/2)$, which corresponds to a point source at the centerline, the coefficient of the τ^3 term also vanishes. This calculation shows the fundamental difference in the short time transitional time scales between point sources at and off the centerline and non-point-source data such as a uniform distribution. In the next section, we will see the application of formula (4.14) to a uniform distribution across only part of the channel.

To summarize, the short time behavior of the enhanced diffusivity for point source release at Z_0 is

$$\frac{\kappa_{\mathit{eff}}}{\kappa} \approx 1 + \frac{32\mathrm{Pe}^2}{3}\left[2\left(Z_0 - \frac{1}{2}\right)^2 \tau^2 + \tau^3\right] \tag{4.17}$$

for a channel between (0,1). Notice that the first quadratic correction term agrees with the expansion (3.32) of the exact variance without free space approximation, showing that the Gaussian kernel is a reasonable approximation when the short time transitional effects occur. For a pipe,

$$\frac{\kappa_{\mathrm{eff}}}{\kappa} \approx 1 + \frac{4\mathrm{Pe}^2}{3}(R_0^2\tau^2 + \tau^3). \tag{4.18}$$

The anomalous scaling suggested by these two formulas agrees with those in Latini and Bernoff.

For transversely uniform initial distribution and quadratic shear, applying the averaging over the width of the channel reads as

$$\frac{\kappa_{\text{eff}}}{\kappa} \approx \begin{cases} 1+\dfrac{16\text{Pe}^2}{3}\Big(\dfrac{\tau}{120}+\dfrac{\tau^2}{3}+2\tau^3\Big), & \text{Channel,} \\ 1+\dfrac{\text{Pe}^2}{3}\Big(\dfrac{\tau}{8}+2\tau^2+4\tau^3\Big), & \text{Pipe.} \end{cases} \tag{4.19}$$

These approximations only agree with the asymptotic relations (3.24) and (4.10) derived from the exact kernel up to the linear correction term, which yields the transition time scale to the anomalous regime. This should be expected since the boundary effects are significant almost immediately for the particle near the walls for the transversely uniform data. Figure 4.2 evaluates the accuracy of the higher order correction of these Gaussian approximations compared to the exact enhancement (3.22). Here we can clearly see that the 4-term, free-space estimate on the left fails much sooner than the analogous exact kernel asymptotics.

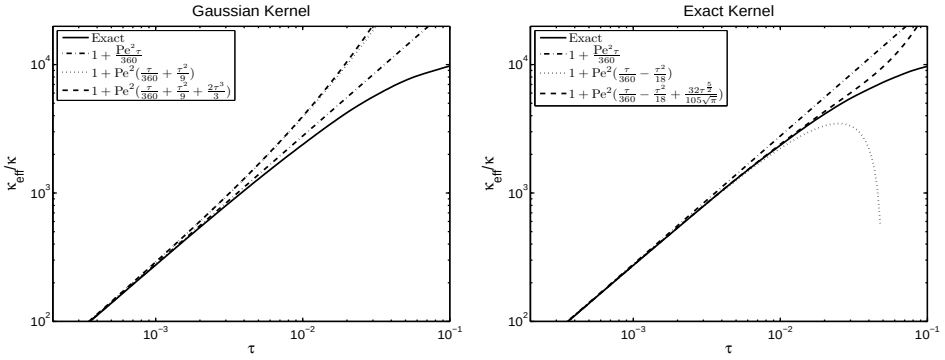

Fig. 4.2: Gaussian kernel asymptotics vs exact kernel asymptotics when $\text{Pe}=2500, T_0(x,z,\tau)\equiv\bar{T}_0(x)$ in a channel.

4.4. Strip data. To try to understand how the case of transversely uniform initial data arises from the case involving an initial condition which is a spanwise delta function, we return to the case of channel flow, and derive an expression for the scalar variance for the special case of initial data on a centered strip.

To connect the two different anomalous time scalings (3.24) and (3.25), we consider the initial data $T_0(x,z)=\bar{T}_0(x)H(z-\frac{a}{2}(1-w))H(\frac{1}{2}(1+w)-z), 0<w<1$, where H is the Heaviside function. With this data, Z_0 is uniformly distributed in $[\frac{1}{2}(1-w),\frac{1}{2}(1+w)]$. Consequently, the limit $w\to 1$ formally corresponds to the transversely uniform data, whereas $w\to 0$ corresponds to a point source at $z=\frac{1}{2}$. The flow-enhanced diffusion with this initial data is

$$\begin{aligned}\frac{\kappa_{eff}}{\kappa} &= \frac{\big\langle X(\tau)^2\big\rangle_\omega - \big\langle X(\tau)\big\rangle_\omega^2}{2\tau} \\ &= 1+\frac{2\text{Pe}^2}{\pi^6}\sum_{n=1}^{\infty}\frac{1}{n^6}\left[1+\frac{e^{-4n^2\pi^2\tau}-1}{4n^2\pi^2\tau}\right]+\frac{\text{Pe}^2}{\pi^7 w\tau}\sum_{m,n=1}^{\infty}\frac{\cos(n\pi)\sin(n\pi w)}{n}K_{mn}(\tau)\end{aligned}$$

$$-\frac{2\mathrm{Pe}^2}{3\pi^5 w}\sum_{n=1}^{\infty}\frac{\cos(n\pi)\sin(n\pi w)}{n^5}\left[e^{-4n^2\pi^2\tau}+\frac{e^{-4n^2\pi^2\tau}-1}{4n^2\pi^2\tau}\right]$$
$$-\frac{\mathrm{Pe}^2}{2\pi^{10}w^2\tau}\Big[\sum_{n=1}^{\infty}\frac{\cos(n\pi)\sin(n\pi w)}{n^5}\big(e^{-4n^2\pi^2\tau}-1\big)\Big]^2 \tag{4.20}$$

since

$$\frac{1}{w}\int_{\frac{1}{2}(1-w)}^{\frac{1}{2}(1-w)}\cos(2n\pi z)dz=\frac{\cos(n\pi)\sin(n\pi w)}{n\pi w}, \tag{4.21}$$

and the short time asymptotic behavior obtained by free-space, Gaussian kernel approximation reads

$$\frac{\kappa_{\mathrm{eff}}}{\kappa}\approx 1+\frac{16\mathrm{Pe}^2}{3}\Big(\frac{w^4\tau}{120}+\frac{w^2\tau^2}{3}+2\tau^3\Big),\quad \tau\to 0. \tag{4.22}$$

Therefore, the $w\to 0$ limit of the above formula converges formally to (4.17), the

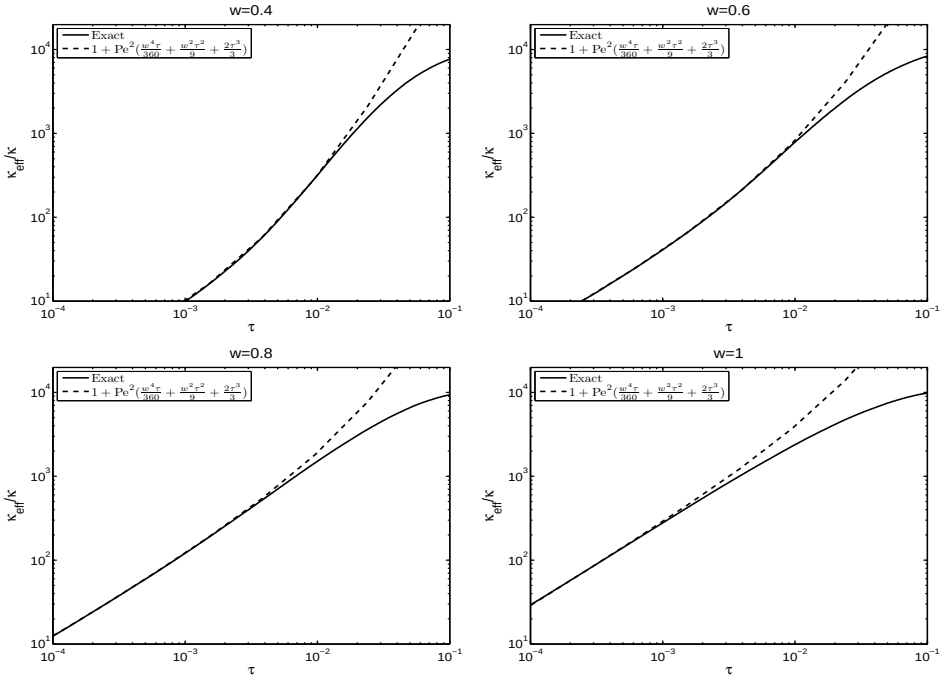

Fig. 4.3: Gaussian kernel asymptotics for
$T_0(x,z)=\overline{T}_0(x)H(z-\frac{1}{2}(1-w))H(\frac{1}{2}(1+w)-z)$.

predictions using the free space Gaussian kernel with $Z_0=\frac{1}{2}$. However, as we saw in figure 4.2, this estimate will deteriorate with increasing w, which is demonstrated in figure 4.3 where this estimate is compared with the exact value (4.20) for different values of w. Observe that as w increases, the timescale of agreement between the exact formula and the free space approximation deteriorates, agreeing on shorter and shorter timescales with increasing strip width.

5. Higher order statistics

Besides the variance of scalar particles, which is directly related to the enhanced diffusivity, the skewness and the kurtosis of the particle distribution is also of considerable interest [8, 20]. The correlation formula (3.11) can also be applied to compute averages like $\langle (x - X_0)^3 \rangle_\omega$ and the averaging calculations are very similar but more tedious than those for the variance, and we defer those calculations for future work. Nonetheless, it is interesting to consider if the anomalous and Taylor timescales derived in the second moment correspond to the timescales on which the passive scalar may develop a non-zero skewness. To this end, we perform some preliminary Monte-Carlo particle simulations of the SDE formulation. The details of these simulations are outlined in the Appendix. We find that the evolution of the skewness and of the kurtosis also exhibit phase transitions from the initial diffusive regime to an anomalous, ballistic regime with a negative skewness and a smaller kurtosis than Gaussian, and finally settle in the Taylor regime. Moreover, these transitions occur at exactly the same time scales suggested by the asymptotic formulas (3.21), (3.25), (4.9), and (4.11) for the variance. For example, figure 5.1 shows the evolution of the particle skewness in the channel dispersion, which has a region of negative values between $\tau_1 \approx \left(\frac{3}{32\mathrm{Pe}^2}\right)^{1/3} \approx 2.5 \times 10^{-3}$ (centerline point data) or $\tau_1 \approx \frac{360}{16}\mathrm{Pe}^{-2} = 3.6 \times 10^{-6}$ (transversely uniform data) and $\tau_2 \approx 0.25$, suggesting an asymmetric probability density function for the displacement $X(\tau)$ of a particle, while when $\tau \lesssim \tau_1$ or $\tau \gtrsim \tau_2$, the density function is symmetric with vanishing skewness. These time scales are identical to those observed in figure 3.2. Therefore, one future direction of our research will involve the derivation of the exact formula for the skewness and the kurtosis in Taylor dispersion, similar to the variance formulas (3.20) and (4.6).

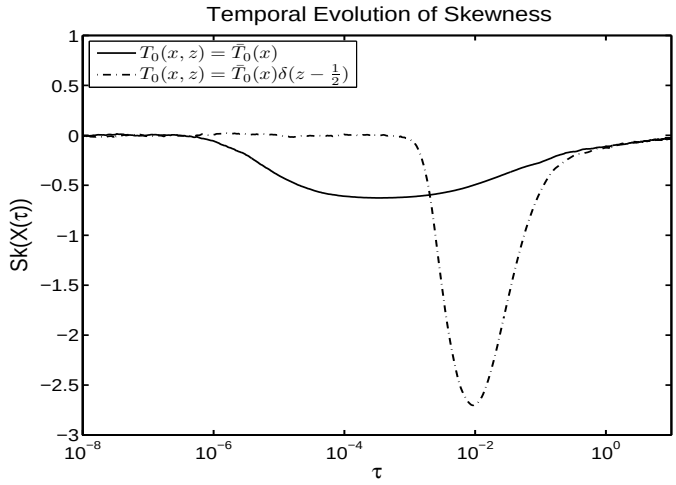

Fig. 5.1: The evolution of the skewness in channel dispersion when $\mathrm{Pe} = 2500$ which shows the identical transitional time scales as the variance.

6. Conclusion

Using the stochastic differential equations underlying the passive scalar in the presence of pipe and channel flow, appealing to the available single point probability function for bounded Brownian motion with vanishing Neumann boundary conditions, along with use of conditional probabilities to compute the needed temporal correla-

tions, we have found new formulas for the exact evolution of the scalar variance. These formulas connect the anomalous transport regime to the long Taylor dispersion regime, and also simplify dramatically when the initial distribution is transversely uniform. Further, the formulas show situations under which free space methods which neglect the boundary conditions successfully model the anomalous regime. It is noteworthy that the free space methodologies employed by Lighthill and Latini and Bernoff provide additional information beyond the variance in that they offer the spatial structure as well, despite the fact that the boundary conditions are violated. Of course, the methodologies employed here using the stochastic differential equation will offer the same information by direct computation of the free space path integral connecting the stochastic trajectories to the passive scalar solution. Andy Majda utilized free space path integrals in several important contexts involving flows with random coefficients. With these tools, he was able to derive exact statistical moment equations for the random passive scalar [13], which in some cases can even be solved in closed form showing situations in which the inherited scalar probability distribution may evolve into a non-Gaussian distribution [14, 16]. In our current work, we are investigating the use of path integrals for the much different case involving *bounded* Brownian motion which may uncover new features of passive scalar transport.

Appendix A. Computing the integrals $\int_{[0,\tau]^2}\langle Z^2(s)Z^2(s')\rangle_\omega dsds'$ and $\int_{[0,\tau]^2}\langle Z^2(s)Z(s')\rangle_\omega dsds'$. These averages can be decomposed as in (3.16), and the explicit formulas for these integrals are

$$\begin{aligned} I_{21} &= 8\int_0^\tau ds'\int_0^{s'} ds\int_0^1 dx\Big[\frac{x^2}{12}+x^2\sum_{m=1}^{\infty}\frac{(-1)^m}{m^2\pi^2}\cos(m\pi x)e^{-m^2\pi^2(s'-s)}\Big]\\ &= \frac{\tau^2}{9}+\frac{16}{\pi^8}\sum_{m=1}^{\infty}\frac{m^2\pi^2\tau+e^{-m^2\pi^2\tau}-1}{m^8}, \end{aligned}$$

$$\begin{aligned} I_{22} &= \frac{4}{3}\int_0^\tau ds'\int_0^{s'} ds\int_0^1 dx\Big[x^2\sum_{n=1}^{\infty}\cos(n\pi x)\cos(n\pi Z_0)e^{-n^2\pi^2\tau}\Big]\\ &= \frac{8}{3\pi^6}\sum_{n=1}^{\infty}\frac{(-1)^n}{n^6}\cos(n\pi Z_0)\big(n^2\pi^2\tau+e^{-n^2\pi^2\tau}-1\big), \end{aligned}$$

$$\begin{aligned} I_{23} &= 16\sum_{m,n=1}^{\infty}\frac{(-1)^m}{m^2\pi^2}\cos(n\pi Z_0)\int_0^\tau ds'\int_0^{s'} ds\int_0^1 dx\Big\{x^2\cos(m\pi x)\\ &\quad\times\cos(n\pi x)e^{-m^2\pi^2(s'-s)-n^2\pi^2\tau}\Big\}\\ &= \frac{32}{\pi^8}\sum_{m,n=1}^{\infty}\frac{(-1)^n(m^2+n^2)}{m^4n^2(m^2-n^2)^3}\cos(n\pi Z_0)\Big[m^2(1-e^{-n^2\pi^2\tau})+n^2(e^{-m^2\pi^2\tau}-1)\Big], \end{aligned}$$

$$I_{31} = I_{34} = 2\int_0^\tau ds' \int_0^{s'} ds \int_0^1 dx \Big[\frac{x^2}{4} + x^2 \sum_{m=1}^{\infty} \frac{(-1)^m - 1}{m^2\pi^2} \cos(m\pi x) e^{-m^2\pi^2(s'-s)}\Big]$$
$$= \frac{\tau^2}{12} + \frac{4}{\pi^8} \sum_{m=1}^{\infty} \frac{1-(-1)^m}{m^8} [m^2\pi^2\tau + e^{-m^2\pi^2\tau} - 1],$$

$$I_{32} = \int_0^\tau ds' \int_0^{s'} ds \int_0^1 dx \Big[x^2 \sum_{n=1}^{\infty} \cos(n\pi x)\cos(n\pi Z_0) e^{-n^2\pi^2\tau}\Big]$$
$$= \frac{2}{\pi^6} \sum_{n=1}^{\infty} \frac{(-1)^n}{n^6} \cos(n\pi Z_0)(n^2\pi^2\tau + e^{-n^2\pi^2\tau} - 1),$$

$$I_{33} = 4 \sum_{m,n=1}^{\infty} \frac{(-1)^m - 1}{m^2\pi^2} \cos(n\pi Z_0) \int_0^\tau ds' \int_0^{s'} ds \int_0^1 dx \big\{x^2 \cos(m\pi x)$$
$$\times \cos(n\pi x) e^{-m^2\pi^2(s'-s) - n^2\pi^2 s}\big\}$$
$$= \frac{8}{\pi^8} \sum_{m,n=1}^{\infty} \frac{[(-1)^n - (-1)^{m-n}](m^2+n^2)}{m^4 n^2 (m^2-n^2)^3} \cos(n\pi Z_0)$$
$$\times \big[m^2(1 - e^{-n^2\pi^2\tau}) + n^2(e^{-m^2\pi^2\tau} - 1)\big],$$

$$I_{35} = \frac{2}{3}\int_0^1 ds \int_0^s ds' \int_0^1 dx \Big[x \sum_{n=1}^{\infty} \cos(n\pi x)\cos(n\pi Z_0) e^{-n^2\pi^2 s'}\Big]$$
$$= \frac{2}{3\pi^6} \sum_{n=1}^{\infty} \frac{(-1)^n - 1}{n^6} \cos(n\pi Z_0)[n^2\pi^2\tau + e^{-n^2\pi^2\tau} - 1],$$

$$I_{36} = 8 \sum_{m,n=1}^{\infty} \frac{(-1)^m}{m^2\pi^2} \cos(n\pi Z_0) \int_0^\tau ds \int_0^s ds' \int_0^1 dx \Big\{x \cos(m\pi x)$$
$$\times \cos(n\pi x) e^{-m^2\pi^2(s-s') - n^2\pi^2 s'}\Big\}$$
$$= \frac{8}{\pi^8} \sum_{m,n=1}^{\infty} \frac{[(-1)^n - (-1)^m](m^2+n^2)}{m^4 n^2 (m^2-n^2)^3} \cos(n\pi Z_0)$$
$$\times \Big[m^2(1 - e^{-n^2\pi^2\tau}) + n^2(e^{-m^2\pi^2\tau} - 1)\Big].$$

Appendix B. Direct Monte Carlo Simulation. The direct particle simulation of the SDE (3.7) is straightforward and which involves generating sample paths for the Brownian processes W_1 and W_2. For example, figure 5.1 is generated by 10^5 such random paths. W_1 is the classical white noise process on the real line that can be approximated by the discretization $W_1(\tau) \simeq \sum_{i=0}^{N} dw_i$ where $dw_i, i = 0, 1, \ldots$ are i.i.d. Gaussian random variables with the uniform temporal stepsize $\Delta\tau$ (set to be 10^{-10} in our simulations) being the variance. However, $W_2(\tau)$ is the bounded Brownian motion and therefore we need to impose a reflective solid wall boundary condition at 0 and 1. The simulation scheme we adopt is a straightforward Euler scheme [12] to general particle trajectories, in which the position of a particle will be temporally incremented

by a discretized Gaussian white noise process modulo the width of the channel or the radius of the pipe. Consequently, the simulated values of quantities such as $\langle X^2(\tau)\rangle_\omega$ can be obtained by ensemble-averaging the stochastic processes evaluated along these random samples.

Appendix C. RC was partially supported by NSF DMS-0509423 and NSF DMS-0620687. RMM was partially supported by NSF CMG ATM-0327906, NSF DMS-030868, and NSF DMS-0502266. ZL was partially supported by NSF PHY-0555324. The authors thank Jared Bronski, Charlie Doering and Peter Kramer for helpful discussions.

REFERENCES

[1] R. Aris, *On the dispersion of a solute in a fluid flowing through a tube*, Proc. R. Soc. Lond. A, 235(1200), 67–77, 1956.
[2] M. Abramowitz and I.A. Stegun, *Handbook of Mathematical Functions with Formulas, Graphs, and Mathematical Tables*, 9th printing, Dover, New York, 1972.
[3] M. Avellaneda and A.J. Majda, *An integral representation and bounds on the effective diffusivity in passive advection by laminar and turbulent flows*, Commun. Math. Phys., 138(2), 339–391, 1991.
[4] M. Avellaneda and A.J. Majda, *Renormalization theory for eddy diffusivity in turbulent transport*, Phys. Rev. Lett., 68(20), 3028–3031, 1992.
[5] H. Brenner and D.A. Edwards, *Macrotransport Processes*, Butterworth-Heinemann, Boston, 1993.
[6] P.C. Chatwin, *The initial develoption of longitudial dispersion in straight tubes*, J. Fluid Mech., 80, 33–48, 1977.
[7] E. Elizalde, S. Leseduarte and A. Romeo, *Sum rules for zeros of Bessel functions and an application to spherical Aharonov-Bohm quantum bags*, J. Phys. A, 26, 2409–2419, 1993.
[8] M. Latini and A.J. Bernoff, *Transient anomalous diffusion in Poiseuille flow*, J. Fluid Mech., 441, 399–411, 2001.
[9] C.W. Gardiner, *Handbook of Stochastic Methods*, Springer, New York, 2004.
[10] V.V. Jikov, S.M. Kozlov and O.A. Oleinik, *Homogenization of Differential Operators and Integral Functionals*, Springer-Verlag, New York, 1994.
[11] M.J. Lighthill, *Initial Development of Diffusion in Poiseuille Flow*, IMA J. Appl. Math., 2(1), 97–108, 1966.
[12] P.L. Lions and A.S. Sznitman, *Stochastic differential equations with reflecting boundary conditions*, Commun. Pur. Appl. Math., 37(4), 511–537, 1984.
[13] A.J. Majda, *Explicit inertial range renormalization theory in a model for turbulent diffusion*, J. Stat. Phys., 73, 515–542, 1993.
[14] A.J. Majda, *The random uniform shear layer: an explicit example of turbulent diffusion with broad tail probability distributions*, Phys. Fluids A, 5(8), 1963–1970, 1993.
[15] A.J. Majda and P. Kramer, *Simplified models for turbulent diffusion: theory, numerical modelling, and physical phenomenon*, Physics Reports, 314, 237–574, 1999.
[16] R.M. McLaughlin and A.J. Majda, *An explicit example with non-Gaussian probability distribution for nontrivial scalar mean and fluctuation*, Phys. Fluids, 8(2), 536–547, 1996.
[17] R.Smith, *Gaussian approximation for contaminant dispersion*, Q. J. Mech. Appl. Math., 35(3), 345–366, 1982.
[18] G.I. Taylor, *Dispersion of soluble matter in solvent flowing slowly through a tube*, Proc. R. Soc. Lond. A, 219(1137), 186–203, 1953.
[19] C. Vanden-Broeck, *A stochastic description of longitudinal dispersion in uniaxial flows*, Physica, 112A, 343–352, 1982.
[20] W.R. Young and S. Jones, *Shear Dispersion*, Phys. Fluids A, 3(5), 1087–1101, 1991.